

# Electric Sailing under Observed Solar Wind Conditions

P. K. Toivanen and P. Janhunen

Finnish Meteorological Institute, Finland

Received: 4 December 2008 – Accepted: 4 May 2009 – Published: 26 October 2009

**Abstract.** In this paper, sailing and navigation in the solar wind with a spacecraft powered by an electric sail is addressed. The electric sail is a novel propellantless spacecraft propulsion concept based on positively charged tethers that are centrifugally uncoiled and stabilised to extract the solar wind momentum by repelling the solar wind protons. Steering of such a sail ship is realised either by changing the tether voltage or the sail spin plane. To model the solar wind, we use spacecraft observations for the density and wind speed at 1 AU and assume that the speed is constant and density decreases in square of the distance from the Sun. Using the electric sail thrust formula, we describe the sail response to the solar wind variations, especially, the self-reefing effect leading to a smooth spacecraft acceleration even during periods of large densities or fast winds. As a result, the variations of the acceleration are statistically small relative to the density and wind speed variations. Considering the navigation, we adopt an optimal transfer orbit to Mars originally obtained for constant solar wind speed and density. The orbit and associated sail operations including a coasting phase are then used as the navigation plan to Mars. We show that passive navigation based only on the statistical results is far too inaccurate for planetary missions and active navigation is required. We assume a simple active navigation system that monitors only the actual orbital speed with an onboard accelerometer and matches it with the optimal orbital speed by altering the tether voltage independently from the future solar wind conditions. We launch 100 test spacecraft with a random launch date and show that with the active navigation 85% (100%) of the spacecraft reach a distance relative to Mars less than about 10 (70) Mars radii with a residual speed less than 20 m/s (80 m/s). As a conclusion, the electric sail is highly navigable and it suits for targeting planets and asteroids, in addition to broad targets such as the heliopause.

## 1 Introduction

The central factor in human space activities is the spacecraft propulsion technology. While chemical rockets are the traditional option used in planetary atmospheres and in space, there is a wide range of concepts proposed for future space-borne propulsion. An intriguing subset of these aims to use the ambient interplanetary energy originating from the Sun either in form of the solar radiation (solar sails) or solar wind. The solar wind as the source of spacecraft thrust was first proposed by Zubrin and Andrews (1991): A magnetic bubble or an artificial magnetosphere generated around the spacecraft deflects the solar wind flow harnessing its momentum. Alternatively, the solar wind can be deviated by an electric field as suggested by (Janhunen, 2004) in terms of an electric sail.

The electric sail is realised with a set of long positively charged tethers emanating from the spacecraft (Janhunen and Sandroos, 2007). The tethers are stabilised by the spacecraft rotation. As the solar wind ions are repelled by the positive tethers, the solar wind momentum is extracted for the spacecraft thrust. The positive tether voltage ( $\sim$  tens of kV) is maintained by an electron gun powered by solar panels. Instead of single wires, multiline tethers (Hoyt and Forward, 2001) are used for an enhanced sail life time against micrometeoroid impacts. Typically, a four-line tether is considered. It has two parallel lines with the other two zigzagging in opposite phase between the parallel ones.

The electric sail is set by unwinding the tethers centrifugally by spinning the spacecraft with chemical thrusters or other arrangements. After the sail is set, the thrusters can be jettisoned. The steering of the sail is similar to that of flying a helicopter as the tether voltage is analogous to the attack angle of the helicopter blades. The level of thrust can obviously be controlled by the tether voltage, but also the sail spin plane can be altered by modulating the tether voltage synchronically with the sail rotation.

As shown by Janhunen and Sandroos (2007), under average solar wind conditions at 1 AU, a force of  $\sim 5 \times 10^{-8}$  N/m



Correspondence to: P. K. Toivanen  
(petri.toivanen@fmi.fi)

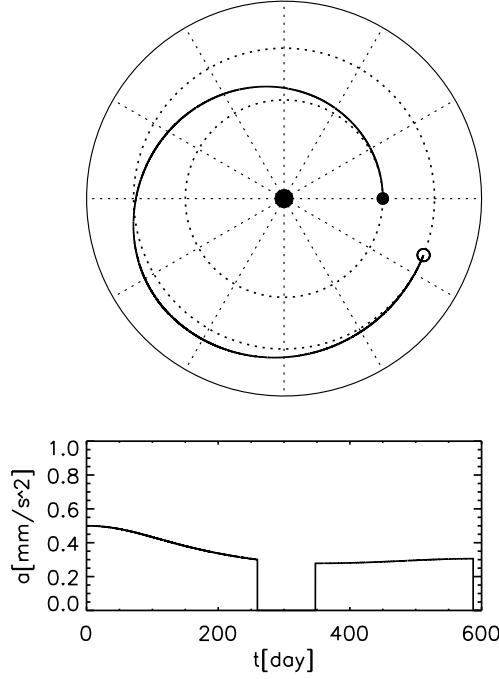


**Fig. 1.** Optimal orbit (top panel) from Earth (solid circle) to Mars (circle) and acceleration (bottom panel) along the orbit according to Mengali et. al. (2008). Note the coasting phase of about 88 days as a key sail operation during the optimal orbit.

per unit tether length can be obtained with the electric sail. A considerable final speed of 50 km/s can, however, be achieved as the tethers are very light consisting of thin ( $\sim$  tens of  $\mu\text{m}$ ) wires. Furthermore, the power requirement for the electron gun is low, and it can be operated with modest solar panel power and mass. Such a large final speed suggests that the electric sail is a promising propulsion concept for missions to the outskirts of the heliosphere, heliopause and Kuiper belt. It also serves as a propellantless propulsion to pull payloads heavier than those of the high-speed missions to planets and to or from asteroids. For such missions, the sail navigation is essential, and as the scope of this paper, we show that the electric sail is highly navigable and suits also for planetary and asteroid missions.

Recently, Mengali et. al. (2008) carried out an electric sail performance analysis assuming average solar wind conditions and radial decay of spacecraft acceleration  $a$  of

$$a = a_0 \left( \frac{r_0}{r} \right)^{7/6}, \quad (1)$$

where  $a_0$  is the spacecraft acceleration at the Earth orbit  $r_0$ , 1 AU. The non-trivial radial decay power of 7/6 arises from four effects (Janhunen and Sandroos, 2007): Decay of the solar wind density; Increase of the effective sail area (increase of the solar wind Debye length); Decay of the electron temperature; and Reduction of the solar panel power. Figure 1 (upper panel) shows the optimal orbit to Mars as obtained

**Table 1.** The electric sail parameters (except  $w_t$ ) adopted from the study of Mengali et. al. (2008). Parameters denoted with \* are not explicitly used in this paper but are shown here for reference. The spacecraft mass-to-power ratio,  $\beta$  is originally adopted from the SMART-1 mission (Milligan et. al., 2006).

Parameter	Definition	Value
$r_w$	Tether wire radius	$10 \mu\text{m}$
$w_t$	Tether width	$2.5 \text{ cm}$
$\rho_w$	Tether wire mass density	$4000 \text{ kg/m}^3$
*	Single tether length	$15.5 \text{ km}$
*	Number of tethers	$100$
*	Solar panel power	$290 \text{ W}$
$\beta$	S/C mass-to-power ratio	$0.25 \text{ kg/W}$
$m_{\text{pay}}$	Payload mass	$100 \text{ kg}$
$\eta$	Payload mass fraction	$0.72$

by Mengali et. al. (2008) as a solution to minimum transfer time problem between circular and coplanar orbits. Using rather conservative assumptions for the electric sail parameters (Table 1), the mission time to Mars is 587 days. This corresponds to an initial acceleration of  $a_0 = 0.5 \text{ mm/s}^2$  at  $r = r_0$  for the values of the solar wind speed (400 km/s), density ( $7.3 \text{ cm}^{-3}$ ), and electron temperature (12 eV) used by Mengali et. al. (2008). Lower panel of Fig. 1 shows the acceleration as a function of time including also a coasting phase of about 88 days as dictated by the optimal solution. Furthermore, the orientation of the sail spin plane was constant at  $20^\circ$ . These sail operations and the optimal orbit are used for studying the effects of the solar wind variations on the orbit and final approach to Mars using either passive or active navigation.

## 2 Electric sail thrust

In general, the acceleration of an electric sail can be defined as

$$a = \frac{(1 - \eta) \sigma_F}{\sigma_{m_b} + \sigma_{m_t}} \quad (2)$$

in terms of the thrust ( $\sigma_F$ ), power unit specific mass (solar panels and electron gun,  $\sigma_{m_b}$ ), and tether specific mass ( $\sigma_{m_t}$ ) all expressed per tether length. Furthermore,  $\eta$  denotes the ratio ( $m_{\text{pay}}/m$ ) of the payload mass ( $m_{\text{pay}}$ ) and total spacecraft mass ( $m = m_b + m_t + m_{\text{pay}}$ ).

Based on the work by Janhunen and Sandroos (2007), the thrust per unit tether length is written as

$$\sigma_F = \frac{6.18 m_p v_{\text{sw}}^2 \sqrt{n \epsilon_0 T_e}}{e \sqrt{\exp \left[ \frac{m_p v_{\text{sw}}^2}{e V} \ln \left( \frac{2}{\sqrt{r_w w_t}} \sqrt{\frac{\epsilon_0 T_e}{n e^2}} \right) \right] - 1}} \quad (3)$$

using the notation of Mengali et. al. (2008). The electric sail variables are tether voltage ( $V$ ), tether wire radius ( $r_w$ ),

and tether width ( $w_t$ ). Here, we have assumed for simplicity that the effective radius of the tether is the geometric average ( $\sqrt{r_w w_t}$ ) of  $r_w$  and  $w_t$  corresponding to the effective radius of a two-line tether (Janhunen and Sandroos, 2007). For tethers with lines more than two, the effective radius and resulting thrust are somewhat larger than those of the two-line tether. Note that Mengali et. al. (2008) used the single wire radius ( $r_w$ ) as the effective tether radius in their study. Solar wind variables in Eq. (3) are solar wind speed ( $v_{sw}$ ), density ( $n$ ), and electron temperature ( $T_e$ ). Natural constants in Eq. (3) are proton mass ( $m_p$ ), vacuum permittivity ( $\epsilon_0$ ), and elementary charge ( $e$ ). Here, it is important to note two key features in the thrust formula Eq. (3): 1) Although the solar wind dynamic pressure is proportional to the density, the thrust is only proportional to  $\sqrt{n}$  since the sail effective area ( $\propto$  electron Debye length) is proportional to  $1/\sqrt{n}$ ; and 2) The dynamic pressure is proportional to  $v_{sw}^2$ , but as the solar wind speed increases, the solar wind ions penetrate deeper into the tether potential structure which limits the increase of the thrust.

The tether mass per unit length in Eq. (2) is given as

$$\sigma_{m_t} = k_t \pi \rho_w r_w^2, \quad (4)$$

where  $k_t$  is a coefficient for a multiline tether ( $k_t = 4.3$ , for a four-line tether) and  $\rho_w$  is the mass density of the tether wire material.

The mass of the power unit consists of those of the solar panels, power processing unit, and electron gun that provide power to support the tether voltage. This power is required to compensate the electric current gathered by the positive tethers as an electron current from the ambient plasma. According to the Langmuir probe theory (Mott-Smith and Langmuir, 1926; and Allen, 1992), the resulting current per unit length ( $\sigma_I$ ) of the tether wire is

$$\sigma_I = 2r_w e n \sqrt{\frac{2eV}{m_e}} \quad (5)$$

assuming that  $eV \gg T_e$  and the electron thermal and bulk velocities are much smaller than  $\sqrt{eV/m_e}$  (Janhunen and Sandroos, 2007). This current corresponds to an ohmic power of  $\sigma_P = \sigma_I V$ . For a reference solar wind density ( $n_0$ ) and maximum tether voltage ( $V_0$ ,  $V < V_0$  in Eq. (3)), the power unit mass per unit tether length in Eq. (2) can be given as

$$\sigma_{m_b} = \beta \sigma_P = 2k_t \beta n_0 r_w \sqrt{\frac{2e^3 V_0^3}{m_e}}, \quad (6)$$

where  $\beta$  is the spacecraft mass-to-power ratio (Mengali et. al., 2008).

A central feature of the electric sail to be added is the tether voltage ( $V$  in Eq. (3)) response to the solar wind density variations. As the mass of the power unit is designed by fixing  $n_0$  and the solar panel power ( $\beta$ ) in Eq. (6), the power unit can support maximum tether voltage ( $V_0$ ) only for density values less than  $n_0$ . For density values larger than  $n_0$ , the tether

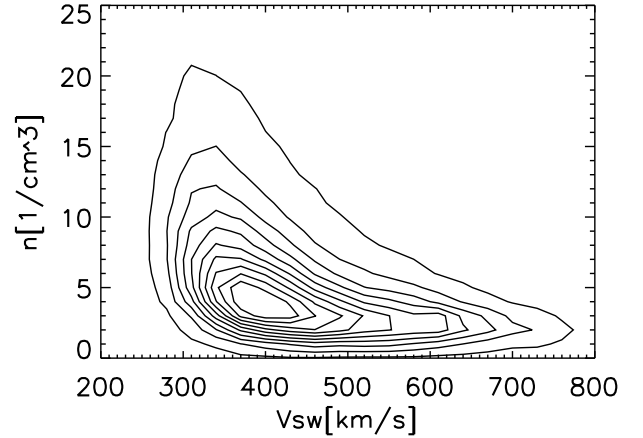


**Fig. 2.** Distribution of the solar wind density and speed (OMNI data with data gaps removed) shown in arbitrary contour levels.

voltage depends on density through the electron current and designed solar panel power. Using Eq. (6) for the actual solar wind density ( $n$ ), the applied tether voltage ( $V < V_0$ ), and the given mass of the power unit ( $\sigma_{m_b}$ ), the tether voltage as a function of the density can be solved to read as

$$V = V_0 \left( \frac{n_0}{n} \right)^{\frac{2}{3}} < V_0. \quad (7)$$

This implies that for densities larger than  $n_0$ , Eq. (3) is not, in practice, proportional to  $\sqrt{n}$  as an increase in density leads also to an increase in the electron current which forces the power system to lower the tether voltage.

### 3 Solar wind data and model

At a given radial distance from the sun, the electric sail thrust depends on the solar wind speed, density, and electron temperature as in Eq. (3). In this paper, we only use solar wind speed and density data and, consequently, focus primarily on these variables. This is mainly because of three reasons: Statistically, the electron temperature does not depend on the wind speed and density (Newbury et. al., 1998); The design of the spacecraft thrust (the reference density and maximum tether voltage in Eq. (7)) is non-trivial only for variations in speed and density; and Statistically, response of the electric sail to electron temperature variations is basically Gaussian. However, the latter two reasons are addressed in the paper when relevant.

The solar wind speed and density measurements are available as OMNI data (King and Papitashvili, 2004) from late 1963 to present. As the solar wind in situ monitoring has not been continuous, there are apparent data gaps in the OMNI data. For the statistical purposes of this paper, the original data is time-stacked by neglecting the data gaps, and since no exact launch windows are considered here, the original timing of the data is irrelevant. This leads to a total of about 29 years

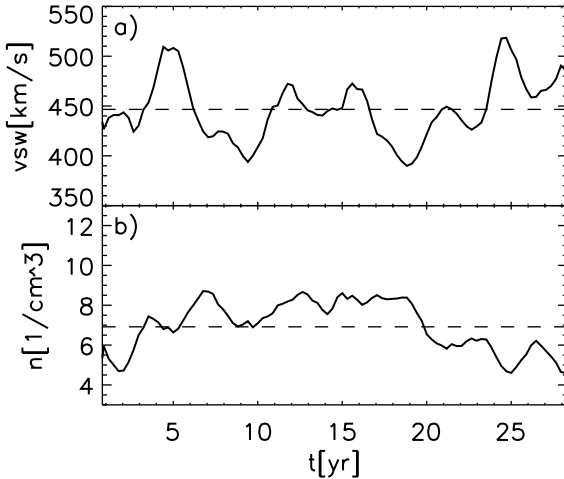


**Fig. 3.** Solar wind (a) speed and (b) density running-averaged over 587 days (time period of the optimal orbit shown in Fig. (1)). The data set used is the OMNI data with data gaps removed (see Sect. 3 for details). The dashed lines indicates the average value of each variable.

of data assumed to represent the solar wind characteristics in this work.

Figure 2 shows the wind speed and density distribution of the OMNI data as reference implying that for high (low) solar wind speed values, the density is typically low (high). In Fig. 3, the data for wind speed and density are running-averaged over 587 days, the optimal orbit period. As indicated by the dashed lines, average values of the wind speed and density over the whole data set are 446.6 km/s and  $6.92 \text{ cm}^{-3}$ , respectively. According to OMNI data, there are time periods long relative to the length of the data set during which either the density or wind speed clearly deviates from the long term averages, a fact that has a key role in designing an electric sailing spacecraft with passive navigation.

In addition to the solar wind data, powers  $p$  of radial profiles of the form  $(r_0/r)^p$  are required to model the solar wind for larger (or smaller) radial distances than 1 AU. In this paper, we adopt the following common values for  $p$ : For the density profile,  $p = 2$ ; wind speed is constant, and  $p = 0$ ; and the electron temperature radial dependence is such that  $p = 1/3$  (Sittler and Scudder, 1980). These values lead to the radial decay of the acceleration as given in Eq. (1). To complete the model, we use an average value of 12.15 eV for the electron temperature as obtained by (Newbury et. al., 1998).

#### 4 Electric sail design

Based on the averaged solar wind speed and density data (Fig. 3), it can be expected that actual electric sail orbits deviate from the optimal orbit depending on the underlying solar wind conditions. In order to study such orbital deviations and their dependence on the designed maximum tether voltage, the electric sail is designed in such a way that its initial

acceleration is  $0.5 \text{ mm/s}^2$  corresponding to the optimal orbit (Fig. 1) independently of the designed maximum tether voltage. In this paper, we consider tether voltages of 20, 30, and 40 kV in addition to that of 10 kV used by Mengali et. al. (2008). The initial acceleration of  $0.5 \text{ mm/s}^2$  can easily be achieved for all tether voltages by using the mass breakdown of Mengali et. al. (2008) (Table 1) and decreasing the payload mass fraction to take into account the power unit mass required by tether voltage levels higher than 10 kV.

Figure 4 shows the spacecraft acceleration profiles for the four selected tether voltages as functions of density, wind speed, and electron temperature. Here, the payload mass fractions are 0.82, 0.80, 0.76, 0.70 leading the optimal acceleration of  $0.5 \text{ mm/s}^2$  for the tether voltages of 10, 20, 30, and 40 kV, respectively. The reference value for the solar wind density ( $n_0$ ) is  $3.4 \text{ cm}^{-3}$  fixing the power unit so that it is working with full power 75% of the time (for 25% of the time,  $V = V_0$ ). For the solar wind speed (electron temperature), the mean (average) value of 421 km/s (12.15 eV) is used. Note that the payload mass fractions given above take also into account the reference solar wind values different from those used by Mengali et. al. (2008). For each panel, one of the solar wind parameters is variable, while the other two are kept constant at their reference values. In addition, Fig. 4 shows the distributions of the density and wind speed as deduced from the OMNI data, and also, as a reference, the electron temperature distribution as adopted from Newbury et. al. (1998).

As a function of density, the acceleration increases for densities less than the reference value of  $3.4 \text{ cm}^{-3}$  approaching to the optimal acceleration of  $0.5 \text{ mm/s}^2$ . For these density values, the tether voltage is at the maximum ( $V_0$  in Eq. (7)), and no effect of the voltage on the acceleration can be identified because of its scaling by the payload mass fraction. For the densities higher than the reference density, the available voltage decreases (as  $V$  in Eq. (7)) following the increase of the electron current to the tethers, and the acceleration is relatively constant, except for the designed maximum voltage of 10 kV.

In the case of the solar wind speed being the variable, the acceleration profiles are vastly different from each other depending on the designed maximum tether voltage. For the wind speed values less than the mean speed, the lowest applied tether voltage gives the largest acceleration (payload mass fraction scaling effect). For the wind speed values larger than the mean speed, the non-monotonic response of the acceleration to the tether voltage leads to highly reduced acceleration for the voltage of 10 kV but to a significant increase for the voltages larger than 10 kV. Physically, such a behaviour arises from Eq. (3) as the potential structure around the tethers can withstand the penetration of the solar wind ions (with an energy  $\propto m_p v_{\text{sw}}^2$ ) better for high voltages ( $eV > m_p v_{\text{sw}}^2$ ) than for low voltages. This effect together with the voltage dependence on the densities ( $> n_0$ ; Fig. 4) leads to the self-reefing behaviour of the electric sail.

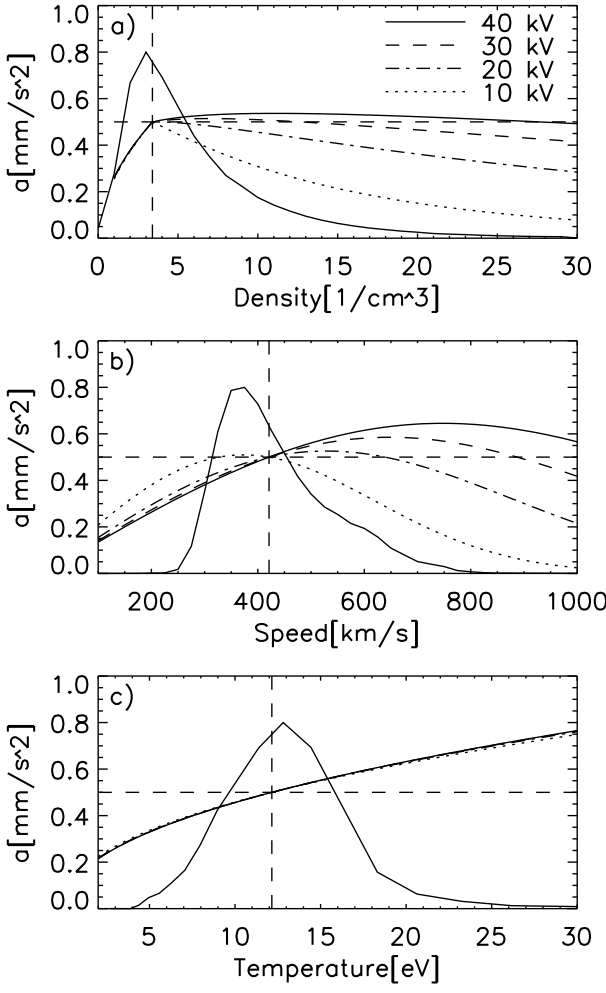


**Fig. 4.** Spacecraft acceleration profiles for four levels of maximum tether voltage as functions of (a) density, (b) wind speed, and (c) electron temperature. The payload mass fractions are 0.82, 0.80, 0.76, 0.70 corresponding to the tether voltage values of 10, 20, 30, 40 kV, respectively. For each of the variables, the dashed vertical lines show the reference values used in electric sail design. In addition, the distribution functions of the respective variables are shown with solid lines in arbitrary units.

Finally, Fig. 4c shows the acceleration profiles as a function of the electron temperature. As it can be seen, the profiles are monotonic throughout the observed temperature range and they are basically independent of the tether voltage used (payload mass fraction scaling effect). Furthermore, temperature distribution is roughly Gaussian and it can be concluded that the electric sail response to electron temperature variations is statistically far more trivial than in the cases of the density and speed variations.

Based on Fig. 4, it can be expected that the electric sail acceleration is non-linear to solar wind variations and less variable for large tether voltages (self-reefing). Figure 5 shows a ten-day period of OMNI data with extreme density and speed

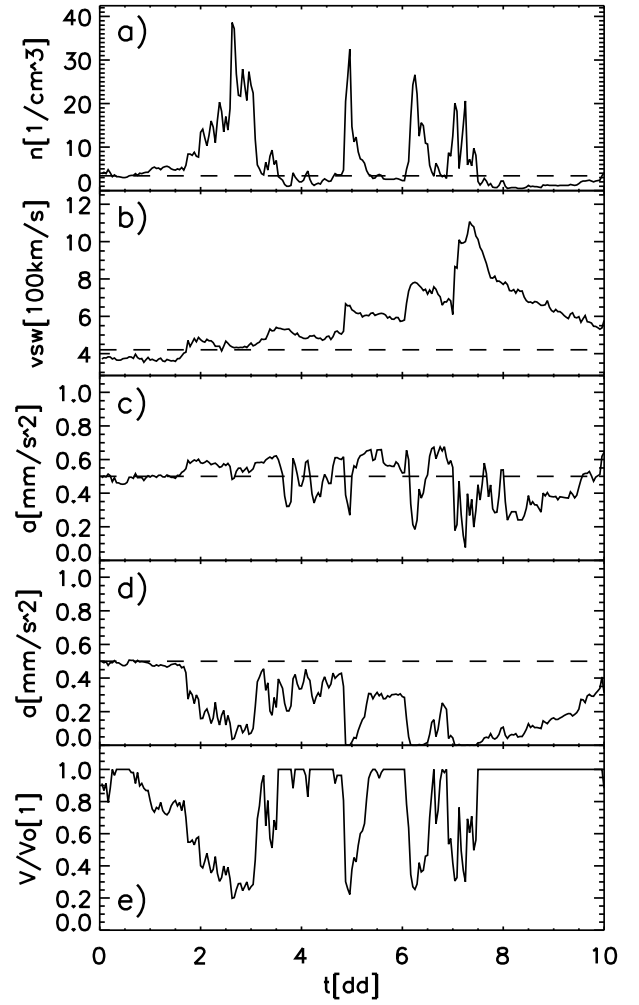


**Fig. 5.** A ten-day period of solar wind data for (a) density and (b) wind speed and resulting acceleration for the maximum voltages ( $V_0$ ) of (c) 40 kV and (d) 10 kV. Panel e shows the instantaneous tether voltage value scaled to the maximum voltage.

variations (panels a and b). For the maximum tether voltage of 40 kV (panel c), the acceleration is far less variable than expected from the density and wind speed variations. This is both because of the sail non-linear response to the wind speed variations and because of the tether voltage decrease (panel e) for large solar wind densities. In the case of the maximum tether voltage of 10 kV, acceleration (panel d) drops for periods of both large wind speeds and densities.

## 5 Statistics of electric sail and passive navigation

The statistical properties such as the distribution and long-term variations of the electric sail acceleration have a key role in sail design. Figure 6 shows the distribution of the acceleration over the OMNI data set. For the cases of the maximum tether voltage larger than 20 kV, the distribution

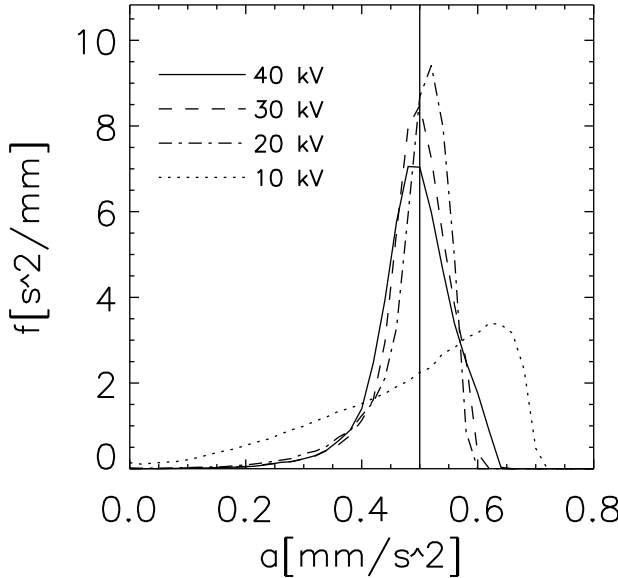


**Fig. 6.** Distribution of the spacecraft acceleration for four levels of the maximum tether voltages. The corresponding payload mass fractions are 0.75, 0.79, 0.76, and 0.72.

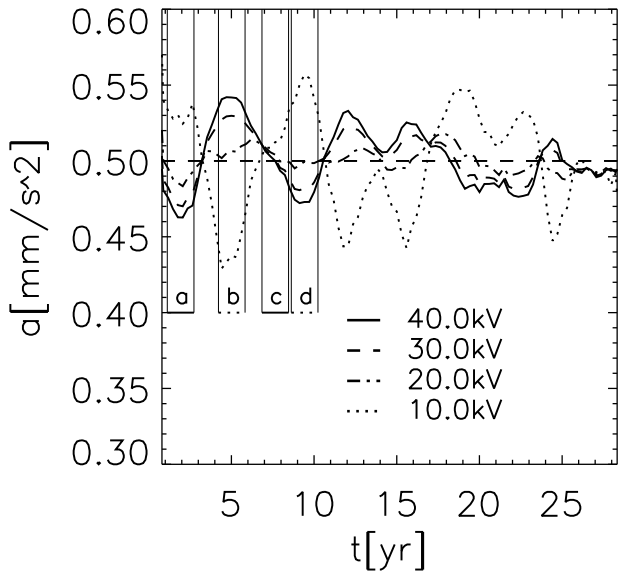


**Fig. 7.** Acceleration of the spacecraft running-averaged over the orbit period (587 days) for four levels of the tether voltage. The solar wind speed and density data set used is the OMNI data with data gaps removed (see Sect. 3 for details). For intervals labeled with 'a', 'b', 'c', and 'd', see Fig. 8.

is basically symmetric and well-peaked around the optimal acceleration. If the voltage is decreased from 20 kV, the distribution becomes strongly asymmetric as seen in the case of the maximum tether voltage of 10 kV. This is caused by the limitation of the acceleration for the density values larger than the reference density (Fig. 4a). The average acceleration

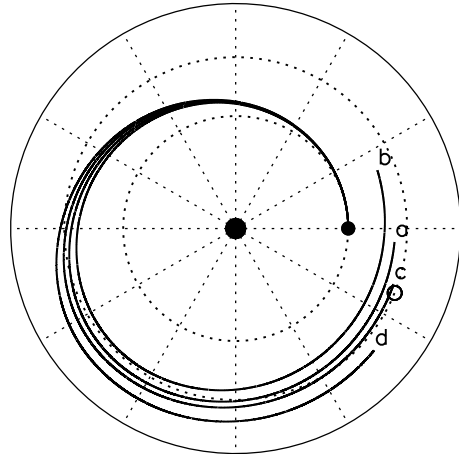


**Fig. 8.** Four example orbits for time intervals shown in Fig. 7 with labels of 'a', 'b', 'c', and 'd'.

for all distributions is the optimum acceleration corresponding to the payload mass fractions of 0.75, 0.79, 0.76, 0.72, for the tether voltages of 10, 20, 30, 40 kV, respectively.

Considering the long-term variations, Fig. 7 shows the acceleration for the four maximum tether voltages averaged over the period of the optimal orbit (587 days). It can be concluded that such variations are small relative to the variations in the solar wind speed and density as shown in Fig. 3. This is the case especially for the maximum tether voltage of 20 kV. An important conclusion to be drawn here is that even during the periods of low acceleration only a small decrease in the payload mass fraction is required to raise the acceleration to the level of the optimum: For the minimum acceleration of about  $0.46 \text{ mm/s}^2$  ( $0.43 \text{ mm/s}^2$ ) for the voltage of 40 kV (10 kV), the payload mass fraction has to be changed from 0.72 (0.75) to 0.70 (0.71).

To conclude the statistical analysis of the passive electric sail navigation, Fig. 8 shows four orbits as examples. These orbits represent four periods of time (Fig. 7) with different levels of averaged acceleration over the orbital period: Minimum accelerations of 0.46 (orbit a) and 0.44 (orbit b) for the tether voltages of 40 kV and 10 kV, respectively; Acceleration of 0.50 (orbit c) with 40 kV; and Maximum acceleration of 0.55 (orbit d) with 10 kV. In all of these cases, the actual orbits deviate significantly from the optimal orbit, and Mars is essentially missed. This is even the case with the optimal average acceleration (orbit c) implying the actual orbit and arrival to Mars is sensitive to the details of the solar wind variations along the spacecraft orbit.

## 6 Active electric sail navigation

The electric sail passive navigation performance can be significantly enhanced by introducing an active orbit control system. Here we assume simply that such a system con-

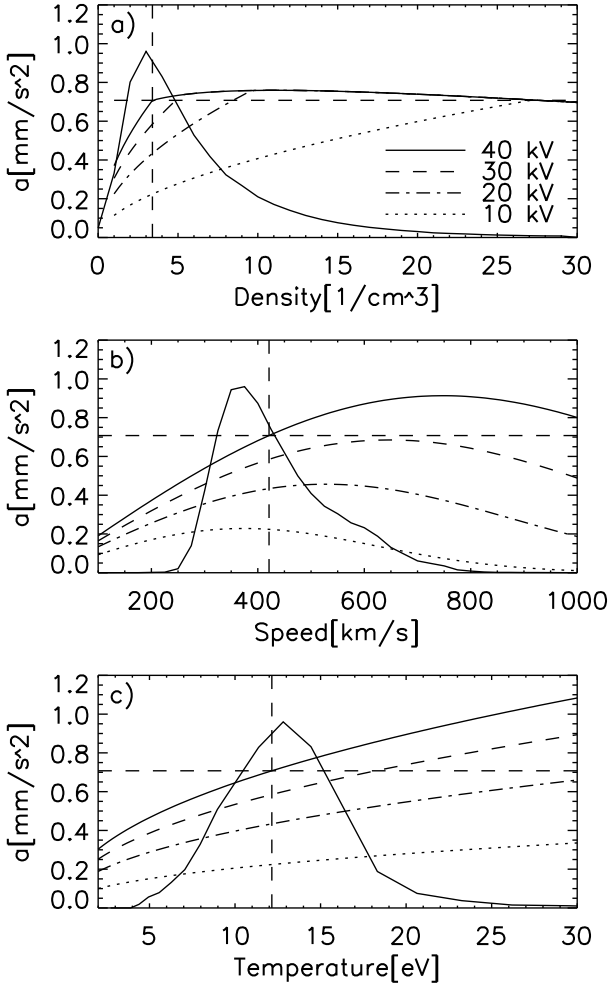


**Fig. 9.** Acceleration of the spacecraft as functions of the solar wind (a) density, (b) speed and (c) electron temperature for four applied tether voltage levels and for fixed payload mass fraction of 0.60. In addition, the distribution functions of the respective variables are shown with solid lines in arbitrary units.

sists of an onboard accelerometer and a control scheme to alter the tether voltage ( $0 < V < V_0$ ) to match the measured orbital speed,  $v_{\text{measured}}$ , time-integrated from the accelerometer data with the optimal orbital speed,  $v_{\text{optimal}}$ , stored in the orbit control system. The control scheme is such that the hourly value of  $v_{\text{measured}}$  is checked against  $v_{\text{optimal}}$  and the tether voltage  $V_t$  is changed to  $V_{t+h}$  for the next hour as

$$\begin{aligned} V_{t+h} &= V_t + \frac{1}{12}V_0 &< V_0, & \text{if } v_{\text{measured}} < v_{\text{optimal}} \\ V_{t+h} &= V_t - \frac{1}{12}V_0 &> 0, & \text{if } v_{\text{measured}} > v_{\text{optimal}}, \end{aligned} \quad (8)$$

independent of the future solar wind conditions. The orbit navigation plan is not changed including the original dates of the coasting phase and the arrival date according to the optimal orbit design.

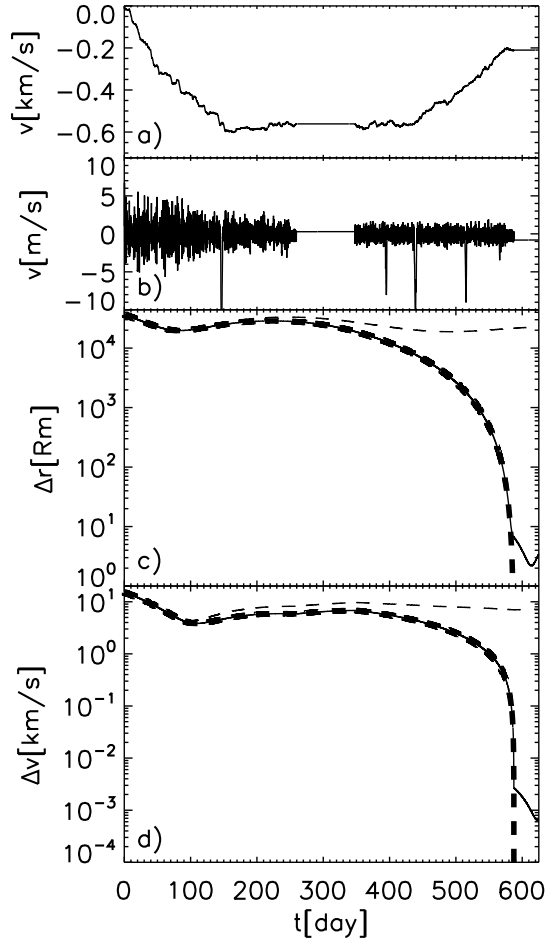


**Fig. 10.** Closest approach to Mars during the orbit with label 'c' in Figs. 7 and 8 (passive navigation) and during an orbit with the active navigation: Error in the orbital speed in the cases of (a) passive and (b) active navigation, (c) distance to Mars and (d) the spacecraft speed relative to Mars as functions of time during the optimal orbit (thick dashed line), during the orbit 'c' (thin dashed line), and during the orbit with active navigation (solid line).

In addition, the payload mass fraction can be decreased to enhance the spacecraft thrust during the periods of low densities. Figure 9 shows the spacecraft acceleration dependence on the applied tether voltage as functions of the solar wind density, speed, and electron temperature. The maximum tether voltage is 40 kV, and the payload mass fraction is 0.60. For example, for the reference density, the acceleration can be varied between zero and about  $0.7 \text{ mm/s}^2$  depending on the applied tether voltage. With the maximum tether voltage, the optimal acceleration level is achieved for densities higher than about  $1.6 \text{ cm}^{-3}$  that is 97% of the OMNI data.

In Fig. 10, the passive and active navigation approaches are compared. Two upper panels show the error in actual orbital speed as a function of time. Two lower panels show the distance to Mars and spacecraft speed relative to Mars both in logarithmic scale. It can be seen that the active naviga-

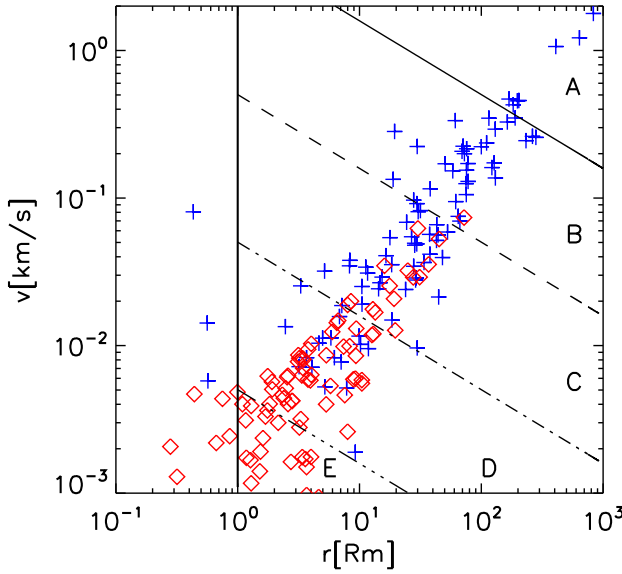


**Fig. 11.** Distribution of the closest approaches to Mars in plane of relative speed and distance to Mars for 100 orbits with random starting date. The maximum tether voltages are 40 kV (red diamonds) and 10 kV (blue plus signs). The solid vertical line indicates the surface of Mars. The four slopes indicate the fraction of the relative speed to the escape velocity at the given distance to Mars for fractions of 1 (solid line), 0.1 (dashed line), 0.01 (dash-dotted line), and 0.001 (dash-triple-dotted line).

tion (solid line) can follow well the optimal solution (thick dashed line) very close (about  $2 R_M$ ) to Mars with a residual speed less than 10 m/s.

In order to study the statistics of the closest approach distance and final speed relative to Mars, we launched 100 test spacecraft to Mars with a random starting date. The closest approach is defined as the minimum of the ratio between the relative spacecraft speed and the Martian escape speed along the orbit. Figure 11 shows the distribution of the closest approach distance and residual speed for the cases of the maximum tether voltages of 40 kV (red diamonds) and 10 kV (blue plus signs). The solid slope shows the escape velocity,  $v_e$ , as a function of the distance from Mars. The rest of the slopes shown with dashed, dash-dotted, and dash-triple-dotted lines give reference velocity levels of  $10^{-1} v_e$ ,  $10^{-2} v_e$ ,  $10^{-3} v_e$ , respectively. The number of the spacecraft in each slot (labeled from A to E) between the reference speeds are shown in Table 2. In addition, for 16 of the spacecraft, the final relative speed is less than 1 m/s (row F in Table 2, but not shown in Fig. 11). Clearly, for the tether voltage of 10 kV, the approach to Mars is far less accurate as for the higher maximum tether voltage (see also Table 2). This is basically because of the distribution of the acceleration (Fig. 6) is much wider than for the maximum voltages higher than 20 kV. Finally, it can be concluded that even the simple active navigation system leads to very promising results in the electric sail navigation.

**Table 2.** Arrival statistics of hundred test spacecraft for two designed maximum tether voltage,  $V_0$ . Rows labeled from A to E give the number of spacecraft in each section of Fig. 11. Row F gives the number of spacecraft with residual speed less than 1 m/s (not shown in Fig. 11).

$V_0$	40 kV	10 kV
A	0	7
B	1	32
C	14	37
D	42	19
E	43	5
F	16	3

## 7 Conclusions

In this paper, we presented the first results on effects of the solar wind variations on the electric sail performance and navigation. Based on the sail thrust formula Eq. (3), the acceleration of an electric sail is far less variable both in short and long time scales than the solar wind density and speed, the key feature of the electric sail performance and navigation. The thrust formula Eq. (3) is based on theory and simulation. Its details could well be inaccurate, if not for other reasons, just because it assumes infinitely long tethers whose potential structures do not overlap. For the characteristic numbers of the electric sail design used here and given in Table 1, the total sail area is reduced by 5%, if the overlapping near the spacecraft was taken into account. This effect can be compensated, for example by longer tethers (by about 0.8 km) or by reducing the payload mass fractions. The conclusions of this paper are based only on the fact that the optimal thrust varies much less than the solar wind parameters and that one can throttle the thrust between zero and the variable maximum value at any point which is trivially true. Therefore the conclusions of this paper do not depend on the details of the electric sail force law.

For given solar wind parameters and given amount of available electric power, there is a voltage which maximises the thrust of the electric sail. This optimal voltage becomes high if the solar wind density is low, because then the current gathered by the tethers is low and the available power is sufficient to keep the tethers at high voltage. The electron gun has also some maximal voltage  $V_0$  as a hardware limitation. If  $V_0$  is high (e.g. 40 kV), the solar wind only rarely becomes so tenuous that the optimal voltage would exceed  $V_0$ .

As Fig. 5 indicates, even large variations in the solar wind density and speed cause only modest variations in the optimal performance of the electric sail, at least when the maximum tether voltage,  $V_0$ , is sufficiently high. There are three main reasons for such self-reefing: 1) When the density  $n$  increases, the solar wind dynamic pressure increases as proportional to  $n$ , but since the electron Debye length (sail ef-

fective area) simultaneously decreases as  $1/\sqrt{n}$ , the electric sail thrust increases only as  $\sqrt{n}$ ; 2) If the solar wind speed  $v_{sw}$  increases, the dynamic pressure increases as  $v_{sw}^2$ , but the solar wind ions also penetrate deeper into the tether potential structure which limits the increase of the thrust; and 3) The increase of the density that would increase the thrust as above ( $\propto \sqrt{n}$ ) in reality increases it less since the density increase also increases the electron current gathered by the tethers forcing the power unit to lower the tether voltage in accordance with the available solar panel power. These reasons imply that an attempt to maximise the thrust at all times by optimising the voltage yields to a thrust level which is not only as high as possible, but also varies remarkably little in comparison with the more dramatic variations of the solar wind parameters.

To study the effects of the solar wind variation on the sail navigation, we used an optimal orbit to Mars originally obtained by Mengali et. al. (2008) for constant solar wind density and speed. This orbit is defined by an initial acceleration of  $0.5 \text{ mm/s}^2$  at the Earth orbit, a coasting phase of about 88 days, and a constant sail spin plane angle of  $20^\circ$ . The resulting orbit period is 587 days. This orbit and sail operations were used as a mission navigation plan to study the accuracy in arrival to Mars as the target. We showed that passive navigation that only relies on statistical properties of the sail acceleration leads to significant deviations from the planned orbit. However, with active navigation, the arrival to the target is very accurate in scheduled mission time with a residual speed clearly below the escape speed at the distance of the closest approach.

In order to accurately navigate to a target, one has to select a thrust profile for the mission which is somewhat smaller than the expected maximal thrust calculated with average or predicted solar wind parameters. Then, most of the time, the planned thrust can be exactly maintained by throttling the electron gun. Nevertheless, during some periods, the solar wind will be weak and the thrust will be smaller than the projected one. In this paper, the sail design was such that this was the case for 3% of the time, and we demonstrated that already a simple navigation algorithm works quite well in maintaining the planned orbit. This algorithm attempts to keep up with the navigation plan by increasing the thrust as soon as possible until the integrated delta-v again agrees with the scheduled one.

There are several ways to improve the simple navigation algorithm used in this paper. The coning angle of the sail can also be modified in addition to the scalar thrust. Instead of simply comparing the accumulated delta-v, the orbit optimisation routine can be rerun from the actual spacecraft location to the target every time the sail falls behind the schedule due to weak solar wind. One could also select a thrust envelope which leaves a progressively larger safety margin when approaching the target. This way the planned thrust level during the final approach can readily be achieved.

When the electric sail was first conceived, we emphasised its potential for missions with a broad target such as the heliopause mission. Because the solar wind varies unpredictably, we considered at that time that the electric sail is inherently weaker in terms of the navigation accuracy than, for example the photon sail which is based on the accurately predictable solar radiation pressure. However, with the results of this paper, the situation has drastically improved. The electric sail is accurately navigable, despite the fact that it is based on the fundamentally unpredictable solar wind. Actually, the electric sail is better navigable than the photon sail in the sense that the electric sail thrust magnitude and direction can be controlled independently of each other, while in the photon sail case inclining the sail causes the thrust magnitude and direction to vary in unison.

*Acknowledgements.* This work was supported by Academy of Finland. The OMNI data were obtained from the GSFC/SPDF OMNIWeb interface at <http://omniweb.gsfc.nasa.gov>. We also want to thank Dr. N. Papitashvili for detailed information about the OMNI data.

Edited by: K. Scherer

Reviewed by: two anonymous referees

## References

- Allen, J. E.: Probe theory - the orbital motion approach, *Physica Scripta*, 45, 497–503, 1992.
- Hoyt, R. and Forward, R. L.: Alternate interconnection Hoytether failure resistant multiline tether, US Pat. 6286788 B1, 2001.
- Janhunen, P. and Sandroos, A.: Simulation study of solar wind push on a charged wire: basis of solar wind electric sail propulsion, *Ann. Geophys.*, 25, 755–767, 2007.
- Janhunen, P.: Electric sail for spacecraft propulsion, *J. Propul. Power*, 20(4), 763–764, 2004.
- King, J. H. and Papitashvili, N. E.: Solar wind spatial scales in and comparisons of hourly Wind and ACE plasma and magnetic field data, *J. Geophys. Res.*, 110, A02209, doi:10.1029/2004JA010804, 2004.
- Mengali, G., Quarta, A. A., and Janhunen, A.: Electric sail performance analysis, *J. Spacecraft Rockets*, 45, 122–129, 2008.
- Milligan, D., Camino, O., and Gestal, D.: SMART-1 electric propulsion: An operational perspective, 9th Intern. Conf. on Space Operations, Rome, AIAA paper 2006-5756, 19–23, 2006.
- Mott-Smith, H. M. and Langmuir, I.: The theory of collectors in gaseous discharges, *Phys. Rev.*, 28, 727–736, 1926.
- Newbury, J. A., Russell, C. T., Phillips, J. L., and Gary, S. P.: Electron temperature in the ambient solar wind: Typical properties and a lower bound at 1 AU, *J. Geophys. Res.*, 103, 9553–2566, 1998.
- Sittler, E. C. and Scudder, J. D.: An empirical polytrope law for solar wind thermal electrons between 0.45 and 4.76 AU: Voyager 2 and Mariner 10, *J. Geophys. Res.*, 85, 5131–5137, 1980.
- Zubrin, R. M. and Andrews, D. G.: Magnetic sails and interplanetary travel, *J. Spacecraft Rockets*, 28, 197–203, 1991.